Electronic Supplementary Material (ESI) for Physical Chemistry Chemical Physics.
This journal is © the Owner Societies 2020

Supplementary Information

Scalable Spectrally Selective Mid-Infrared Meta-Absorbers for Advanced Radiative Thermal Engineering

Xianghui Liu[a], *Qi Chang*[a], *Max Yan*[b], *Xin Wang*[a], *Haiwen Zhang*[a], *Han Zhou*[a]*, *Tongxiang Fan*[a]*

[a] State Key Lab of Metal Matrix Composites, School of Materials Science and Engineering, Shanghai Jiao Tong University, Shanghai, 200240, China
[b] Department of Applied Physics, School of Engineering Sciences, KTH Royal Institute of Technology, Kista, 16440, Sweden
E-mail: hanzhou_81@sjtu.edu.cn, txfan@sjtu.edu.cn

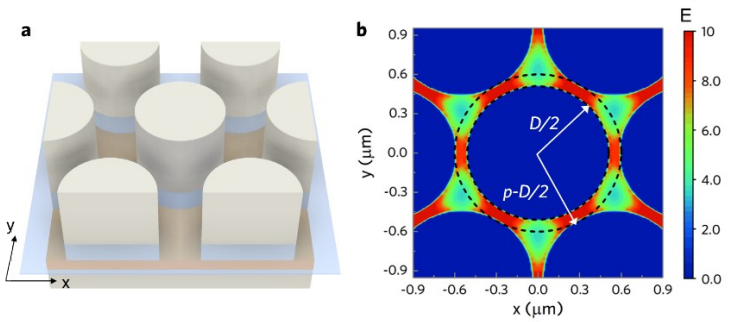

Fig. S1. Simulated average electric filed intensity in the xy plan of meta-absorber with DTR. a), Schematic diagram of the xy plan where we obtained the electric field intensity. b), The simulated electric field intensity in the xy plan of meta-absorber with DTR, which is the average value under TE and TM incident light.

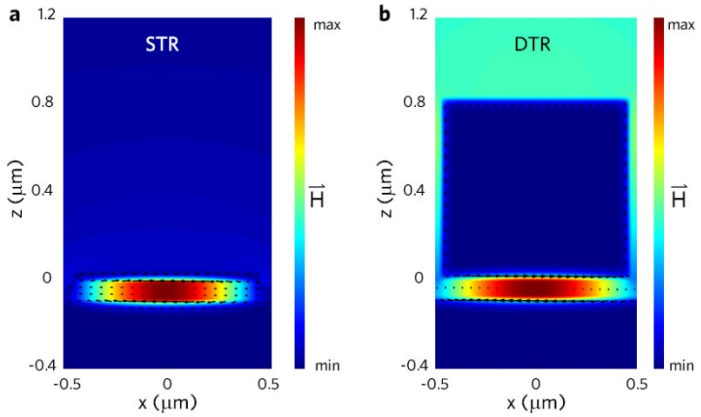

Fig. S2. Antiparallel electric current and confined magnetic field. At resonance, antiparallel electric current or loop electric current is induced for both MIM structures with a) STR and b) DTR, which results in confined magnetic field in Si spacer. The black arrows represent the vectors of current density.

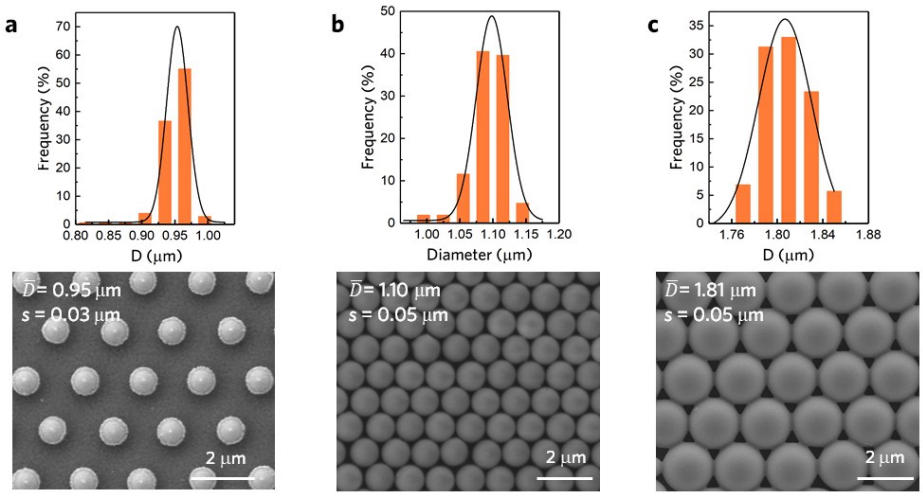

Fig. S3. PS masks used for colloidal lithography. a) Counted diameter distribution and SEM image of the PS masks used for meta-absorber with STR, with average value $\bar{D}$ = 0.95 μm and standard deviation s = 0.03 μm. b) Counted diameter distribution of the PS masks and SEM image used for meta-absorber with DTR, with $\bar{D}$ = 1.10 μm and s = 0.05 μm. c) Counted diameter distribution and SEM image of the PS masks used for creating sparse PS masks in a), with $\bar{D}$ = 1.81 μm and s = 0.05 μm.

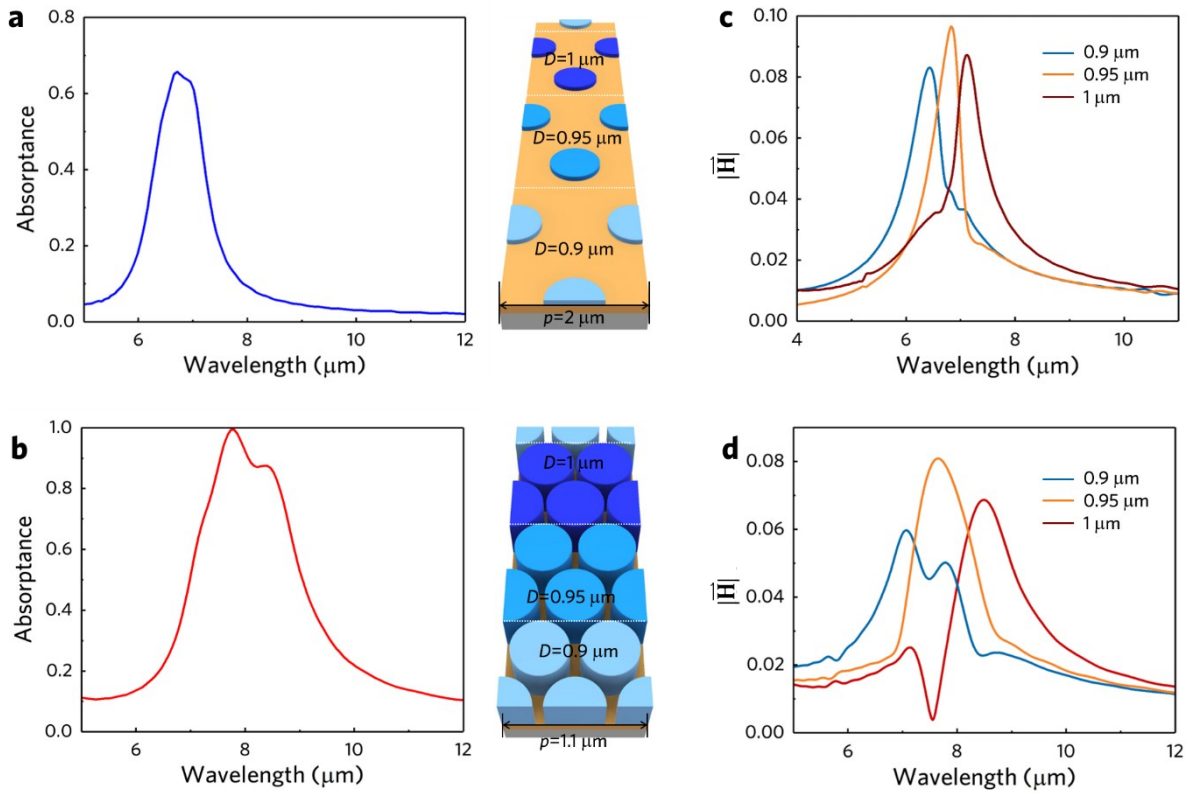

Fig. S4. Comparison of simulated bandwidth between meta-absorbers with STR and DTR. a) and b), Simulated absorptance spectra and MIM structures for meta-absorbers with STR and DTR fabricated by colloidal lithography. For simplicity, only three diameters are selected with values of 0.9 μm, 0.95 μm and 1 μm, in accordance with the maximum, average and minimum within the range. The simulated spectra agree well with our measured results on central wavelength and bandwidth in Fig. 3. c) and d), The magnetic field intensity located in Si spacer under the center of each resonators as functions of wavelength. The magnetic field intensity represents extinction of magnetic resonances. Those three peaks for STR are considerably close and almost overlap with each other. In contrast, they become more disperse and broader for DTR, effectively supporting the claims that even monodisperse DTR generate extended bandwidth.

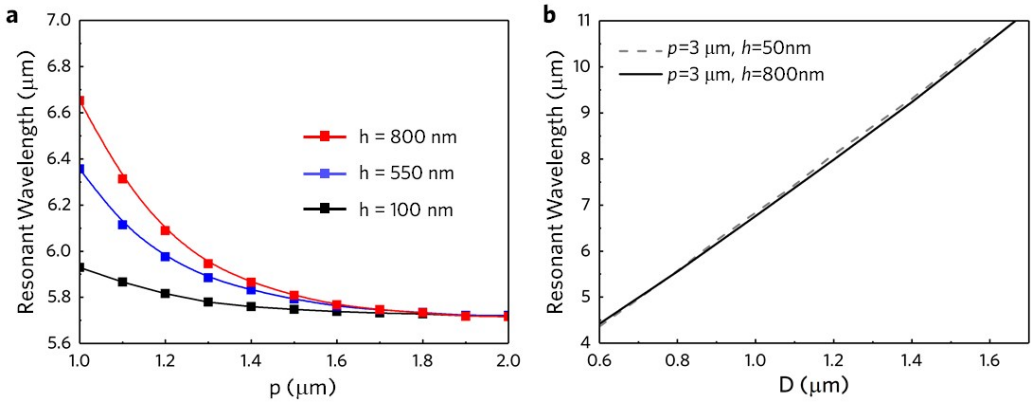

Fig. S5. The effect of *h* and *p* on the resonant wavelength. a) The effect of *p* and *h* on the resonant wavelength of MIM structure. The diameter of resonators and thickness of Si spacer are fixed as 0.8 μm and 60 nm. It can be seen that the redshift of resonant wavelength induced by increasing *h* is obvious only when *p* becomes close to *D*. b) Resonant wavelength changes with increasing of *D* for MIM structures with *p* = 3 μm but different *h*. Because *p* is much larger than *D*, the variation curves are basically similar.

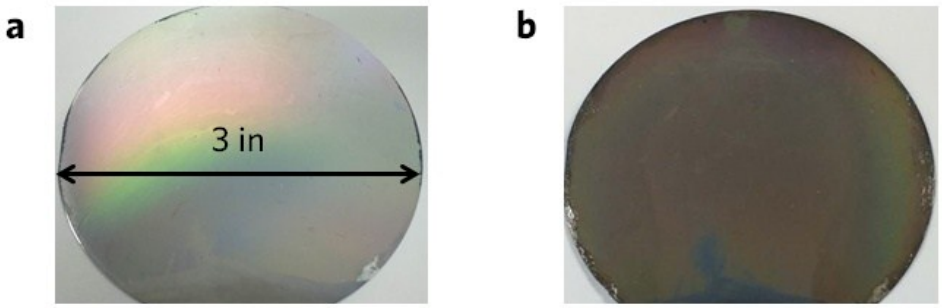

Fig. S6. Digital photos for DTR MA-2 used for radiative cooling. a) DTR MA-2 before RIE. b) DTR MA-2 after RIE.

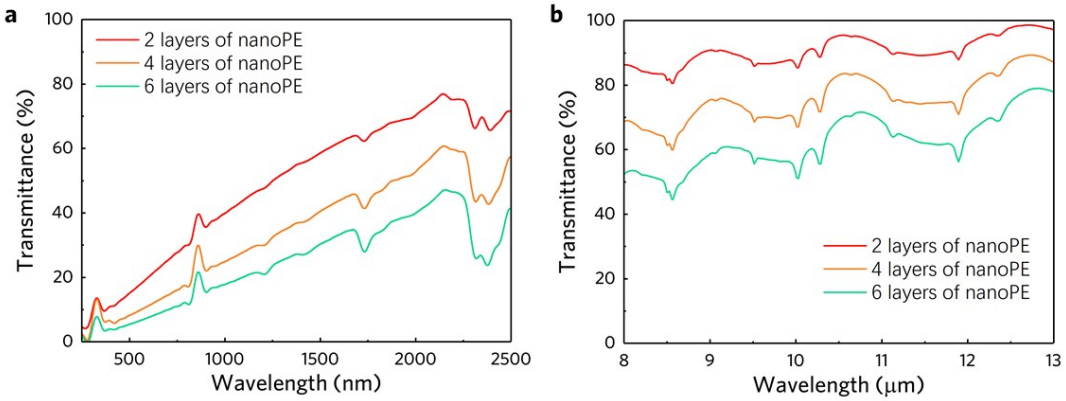

Fig. S7. Optical properties of nanoPE. The transmittance of 2, 4, 6 layers of nanoPE in a) UV-vis-NIR and b) MIR range were measured.

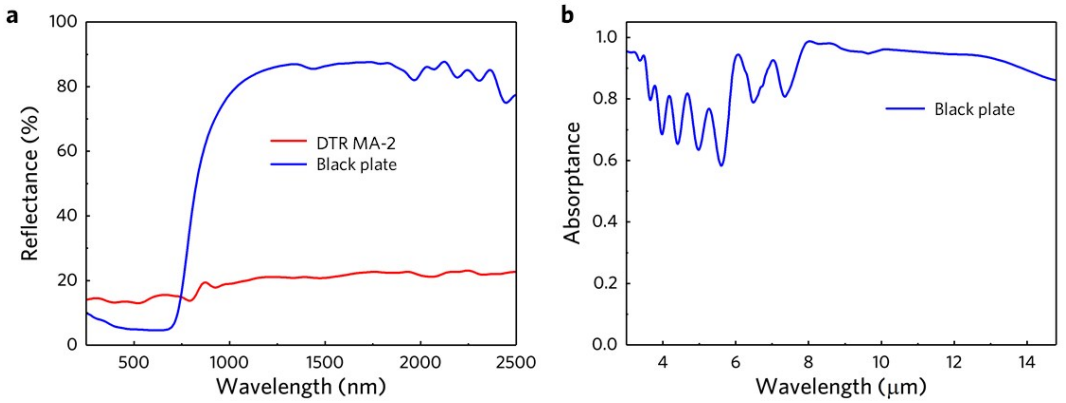

Fig. S8. Optical properties of commercial black plate. a), The reflectance of commercial black plate and DTR MA-2. b), The infrared absorptance of commercially black plate.

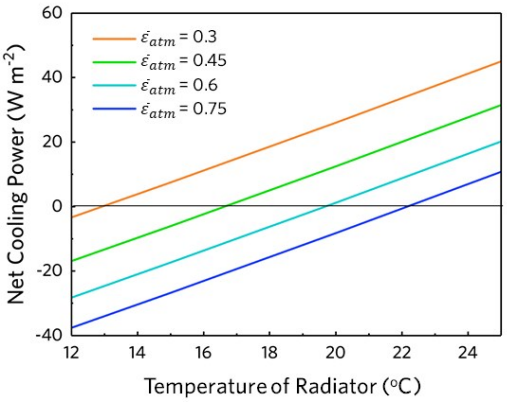

Fig. S9. Influence of relative humidity on the cooling power. The precipitable water vapor concentration that correlated with relative humidity (RH) influences the transparence of

atmosphere significantly. When the precipitable water vapor is 6 cm, $\bar{\varepsilon}_{atm}(0,\lambda)$ increases to about 0.7. This figure shows the change of P_{net} with different $\bar{\varepsilon}_{atm}(0,\lambda)$, the solar radiation is totally removed. As $\bar{\varepsilon}_{atm}$ increasing, P_{net} decreases, which agrees well with the experimental results.

Note S1. Estimating monodisperse diameter distribution.

According to the criterion of the National Institute of Standards and Technology (NIST): "a particle distribution may be considered monodisperse if at least 90% of the distribution lies within 5% of the median size",[1] we derived the relation between mean value and standard deviation through normal distribution as follows.

$$1.65s + \bar{D} < 1.05\bar{D} \tag{S1}$$

1.65 was obtained from normal distribution table when the value of cumulative probability function equals to 0.9505.

So

$$s < 0.0303\bar{D} \tag{S2}$$

Note S2. Derivation of equivalent RLC model.

To further elucidate the broadened spectra, accurate effective impedance needs to be constructed on account of the additional electrical coupling formed by densely arranged resonators. Here we use RLC (resistor-inductor-capacitor) model[2, 3] to describe the relation between resonant wavelength and diameter of resonators. The total impedance Z consists of periodic coupling capacitance (C_g), kinetic inductance (L_e), magnetic inductance or mutual inductance (L_m), and resistance (R_e) of top and ground metal layers as well as gap capacitance of dielectric spacer (C_d)

$$Z = \frac{i\omega(L_e + L_m) + R_e}{1 - \omega^2 C_g (L_e + L_m) + i\omega R_e C_g} + R_e + i\omega(L_e + L_m) + \frac{2}{i\omega C_d} \tag{S3}$$

where ω is angular frequency.

The resistance (R_e) and kinetic inductance (L_e) of metallic layers represent the phase delay in high frequency oscillation, which can be introduced and evaluated from impendence (Z_e) of the material

$$Z_e = \frac{D}{S_{\text{eff}}\sigma} \tag{S4}$$

where S_{eff} is the effective cross section area of induced electric current. To simplify calculation, the shape of induced electric field area in two metal layers was regarded as a square ($D \times D$). Correspondingly, S_{eff} can be expressed as the product of D and skin depth δ. σ is the complex conductivity obtained from Drude conductivity model

$$\sigma = \frac{\varepsilon_0 {\omega_p}^2 \tau}{1 - i\omega\tau} \tag{S5}$$

where τ and ω_p are the relaxation time and plasma frequency of Al ($\tau = 1.02 \times 10^{-14}\,\text{s}$, $\omega_p = 3.145 \times 10^{16}\,\text{Hz}$).[4] Noticing that σ is a complex value, so that Z_e can be divided into real and imaginary parts, which represent R_e and L_e as follows

$$Z_e = \frac{D}{D\delta}\frac{1}{\varepsilon_0 {\omega_p}^2 \tau} - i\omega\frac{D}{D\delta}\frac{1}{\varepsilon_0 {\omega_p}^2} = R_e - i\omega L_e \tag{S6}$$

$$R_e = \frac{1}{\delta}\frac{1}{\varepsilon_0 {\omega_p}^2 \tau} \tag{S7}$$

$$L_e = \frac{1}{\delta}\frac{1}{\varepsilon_0 {\omega_p}^2} \tag{S8}$$

L_m is induced by magnetic energy stored in the dielectric spacer, which can be expressed by the permeability of free space μ_0 and thickness of Si layer d

$$L_m = \frac{1}{2}\mu_0 d \tag{S9}$$

C_d is derived from the capacitance within two parallel charged plates

$$C_d = c'\varepsilon_d\varepsilon_0\frac{\pi D^2}{4d} \tag{S10}$$

where c'=0.26 is a constant that considers fringe effect and non-uniform charge distribution, ε_d is the relative permittivity of Si (ε_d = 3.42).

The real and imaginary parts of Z are

$$\mathrm{Re}\{Z\} = R_e + \frac{R_e}{C_g{}^2 R_e{}^2\omega^2 + [1 - C_g(L_e + L_m)\omega^2]^2} \tag{S11}$$

$$\mathrm{Im}\{Z\} = -\frac{2}{C_d\omega} + (L_e + L_m)\omega + \frac{(L_e + L_m)\omega - C_g R_e{}^2\omega - C_g(L_e + L_m)^2\omega^3}{C_g{}^2 R_e{}^2\omega^2 + [1 - C_g(L_e + L_m)\omega^2]^2} \tag{S12}$$

The resonant frequency (f) can be calculated by zeroing the imaginary part of Z. Notice that the terms containing R_e^2 can be ignored for its too small value. For MIM structure with DTR

$$f = \frac{1}{2\pi}\sqrt{\frac{C_g + C_d - \sqrt{C_g{}^2 + C_d{}^2}}{C_g C_d (L_e + L_m)}}, \text{ for DTR} \tag{S13}$$

For STR, C_g is not considered and the resonant frequency is

$$f = \frac{1}{2\pi}\sqrt{\frac{1}{C_d(L_e + L_m)}}, \text{ for STR} \tag{S14}$$

which is same as to those predicted by previous works.

According to the electric field distribution, we regard the capacitance C_g among resonators as the capacitance between two coaxial cylinders of diameters D and 2p-D with a height h.

The electric intensity between two cylinders is

$$E = \frac{Q}{2\pi\varepsilon_0 hr} \tag{S15}$$

where Q is the total electrical quantity.

The difference of potential is

$$U = \int_{D/2}^{p+D/2} \frac{Q}{2\pi\varepsilon_0 h}\frac{dr}{r} = \frac{Q}{2\pi\varepsilon_0 h}\ln(\frac{2p+D}{D}) \tag{S16}$$

Thus we can obtain the capacitance C_g

$$C_g = \frac{Q}{U} = \frac{2\pi\varepsilon_0 h}{\ln(\frac{2p+D}{D})}. \tag{S17}$$

Note S3. Calculation of radiative cooling power.

As for calculation of net cooling power, the items in Equation 7 can be expressed as follows in detail.

$$P_{rad} = 2\pi \int_0^{\pi/2} \sin\theta\cos\theta \mathrm{d}\theta \int_0^{\infty} \mathrm{d}\lambda \mathrm{I}_{BB}(T_{rad},\lambda)\tau_{\mathrm{cover}}(\theta,\lambda)\varepsilon_{rad}(\theta,\lambda) \tag{S18}$$

$$P_{atm} = 2\pi \int_0^{\pi/2} \sin\theta\cos\theta \mathrm{d}\theta \int_0^{\infty} \mathrm{d}\lambda \mathrm{I}_{BB}(T_{atm},\lambda)\varepsilon_{atm}(\theta,\lambda)\tau_{\mathrm{cover}}(\theta,\lambda)\varepsilon_{rad}(\theta,\lambda) \tag{S19}$$

$$P_{solar} = 2\pi \int_0^{\pi/2} \sin\theta\cos\theta \mathrm{d}\theta \int_0^{\infty} \mathrm{d}\lambda \mathrm{I}_{diffuse}(\lambda)\tau_{\mathrm{cover}}(\theta,\lambda)\varepsilon_{rad}(\theta,\lambda) \tag{S20}$$

$$P_{non} = h_{com}(T_{atm} - T_{rad}) \tag{S21}$$

In above expressions, I_{BB} is the spectral radiance of a black body, T_{rad} is the temperature of absorber, T_{atm} is the temperature of atmosphere. $\varepsilon_{rad}(\theta,\lambda)$ is the emittance of absorber, $\tau_{cover}(\theta,\lambda)$ is the transmittance of covered nanoPE. h_{com} is the combined heat coefficient. Here, ε_{rad} and τ_{cover} are considered as angle independent. $\varepsilon_{atm}(\theta,\lambda)$ is the emittance of atmosphere, estimated by the "box model"[5]

$$\varepsilon_{atm}(\theta,\lambda) = \begin{cases} 1-[1-\overline{\varepsilon}_{atm}(0,\lambda)]^{1/\cos\theta} & \text{for } 8 \le \lambda \le 13\,\mu\mathrm{m} \\ 1 & \text{for } 3 < \lambda < 8\,\mu\mathrm{m} \text{ or } 13 < \lambda < 50\,\mu\mathrm{m} \end{cases} \tag{S22}$$

$\bar{\varepsilon}_{atm}(0,\lambda)$ is the average emissivity of atmosphere at zenith angle and selected as 0.3. $I_{diffuse}$ is the isotropic diffuse-solar spectral radiance. The estimation of $I_{diffuse}$ is referenced to Bikram Bhatia's method[6]

$$I_{diffuse} = I_d \frac{I_0 - I + I_d}{I_0} \tag{S23}$$

$$I_d / I = \begin{cases} 1 - 0.09k & \text{for} k \le 0.22 \\ 0.9511 - 0.1604k + 4.388k^2 - 16.638k^3 + 12.336k^4 & \text{for} 0.22 \le k \le 0.8 \\ 0.165 & \text{for} k > 0.8 \end{cases} \tag{S24}$$

$k=I/I_0$ is the clearness, I is calculated from the AM1.5 solar spectrum, I_0 is calculated from the AM0 solar spectrum. The range of integration is (0.28 μm, 2.5 μm) in solar spectrum and (4 μm, 20 μm) in infrared range.

References

1. Kaye, B. H., *Particle Size Characterization*. Springer US: Boston, MA, 1997; p 1-34.
2. Lee, B. J.; Wang, L. P.; Zhang, Z. M., Coherent thermal emission by excitation of magnetic polaritons between periodic strips and a metallic film. *Opt. Express* 2008, **16**, 11328.
3. Sakurai, A.; Zhao, B.; Zhang, Z. M., Resonant frequency and bandwidth of metamaterial emitters and absorbers predicted by an RLC circuit model. *J. Quant. Spectrosc. Radiat. Transfer* 2014, **149**, 33-40.
4. Palik, E. D., *Handbook of Optical Constants of Solids*. Elsevier: 1985.
5. Granqvist, C. G.; Hjortsberg, A., Radiative cooling to low temperatures: General considerations and application to selectively emitting SiO films. *J. Appl. Phys.* 1981, **52**, 4205-4220.
6. Bhatia, B.; Leroy, A.; Shen, Y.; Zhao, L.; Gianello, M.; Li, D.; Gu, T.; Hu, J.; Soljačić, M.; Wang, E. N., Passive directional sub-ambient daytime radiative cooling. *Nat. Commun.* 2018, **9**, 5001.